Molecular dissection of pheromone selectivity in the competence signaling system ComRS of streptococci

Laura Ledesma-Garcia[a,1], Jordhan Thuillier[b,1], Armando Guzman-Espinola[a], Imke Ensinck[a], Inès Li de la Sierra-Gallay[b], Noureddine Lazar[b], Magali Aumont-Nicaise[b], Johann Mignolet[a], Patrice Soumillion[a], Sylvie Nessler[b,2], and Pascal Hols[a,2]

[a]Louvain Institute of Biomolecular Science and Technology, Biochemistry and Genetics of Microorganisms, Université catholique de Louvain, B-1348 Louvain-La-Neuve, Belgium; and [b]Institute of Integrative Biology of the Cell (I2BC), University Paris-Sarclay, CEA, CNRS, 91198, Gif-sur-Yvette, France

Edited by Emmanuelle Charpentier, Max Planck Institute for Infection Biology, Berlin, Germany, and approved February 20, 2020 (received for review September 16, 2019)

Competence allows bacteria to internalize exogenous DNA fragments for the acquisition of new phenotypes such as antibiotic resistance or virulence traits. In most streptococci, competence is regulated by ComRS signaling, a system based on the mature ComS pheromone (XIP), which is internalized to activate the (R)RNPP-type ComR sensor by triggering dimerization and DNA binding. Cross-talk analyses demonstrated major differences of selectivity between ComRS systems and raised questions concerning the mechanism of pheromone-sensor recognition and coevolution. Here, we decipher the molecular determinants of selectivity of the closely related ComRS systems from *Streptococcus thermophilus* and *Streptococcus vestibularis*. Despite high similarity, we show that the divergence in ComR-XIP interaction does not allow reciprocal activation. We perform the structural analysis of the ComRS system from *S. vestibularis*. Comparison with its ortholog from *S. thermophilus* reveals an activation mechanism based on a toggle switch involving the recruitment of a key loop by the XIP C terminus. Together with a broad mutational analysis, we identify essential residues directly involved in peptide binding. Notably, we generate a ComR mutant that displays a fully reversed selectivity toward the heterologous pheromone with only five point mutations, as well as other ComR variants featuring XIP bispecificity and/or neofunctionalization for hybrid XIP peptides. We also reveal that a single XIP mutation relaxes the strictness of ComR activation, suggesting fast adaptability of molecular communication phenotypes. Overall, this study is paving the way toward the rational design or directed evolution of artificial ComRS systems for a range of biotechnological and biomedical applications.

cell-to-cell communication | quorum sensing | cross-talk | (R)RNPP | XIP pheromone

Competence for natural DNA transformation is a mechanism of horizontal gene transfer that was discovered for the first time in *Streptococcus pneumoniae* (1) but exists in many bacteria (2, 3). This transient physiological state, which generally affects part of the bacterial population, is induced by various environmental stimuli and allows bacteria to internalize exogenous DNA fragments, which could then be integrated into the genome (2–4). Competence provides a high genetic plasticity and facilitates the acquisition of new phenotypic features. Concerning pathogens, competence has been shown to play a role in the evolution of escape mechanisms against the host immune system or in the acquisition of antibiotic resistance genes (5, 6). Competence activation also contributes to the virulence of many streptococci by improving bacterial fitness in the host through bacteriocin production and biofilm formation (7–9).

Competence is regulated at the population level by cell-to-cell communication systems based on secreted signaling molecules (10). Phylogenetic analyses of streptococcal genome sequences and functional studies revealed the existence of two paralogous competence-regulating systems, i.e., the well-characterized ComCDE three-component system (11, 12) and the more recently identified ComRS signaling system (10, 13–17). In contrast to the response regulator ComE, which is indirectly activated by the ComC-derived competence-stimulating peptide through the transmembrane histidine kinase receptor ComD, the sensor ComR is a cytoplasmic competence regulator directly activated by the reinternalized ComS-derived peptide pheromone. ComR belongs to the family of regulators called (R)RNPP for (Rgg), Rap, NprR, PlcR, and PrgX (18, 19), characterized by a C-terminal tetratricopeptide repeat (TPR)-type peptide-binding domain (20) and an N-terminal helix-turn-helix (HTH)-type DNA-binding domain (21). The ComR regulon includes the alternative sigma factor SigX/ComX, which positively regulates genes required for DNA transformation. The activating pheromone, a small linear peptide (7 to 11 amino acids [aa]) derived from the C-terminal part of the ComS precursor, has thus been named XIP for *sigX*/*comX*-inducing peptide (13, 15, 16, 22, 23).

Although the ComRS system is widespread in streptococci groups, sequence analysis has shown an evolutionary divergence of both transcriptional regulator and peptide, suggesting a pheromone-sensor coevolution (10). In the case of ComR, this polymorphism is

Significance

In streptococci, competence for DNA transformation is an adaptive response contributing to genome plasticity and virulence. This process is mainly controlled by the signaling system ComRS, activated through an interaction between the ComS-derived pheromone XIP and the cytoplasmic sensor ComR. ComRS systems evolved divergently and display different preferences for cognate and noncognate XIP peptides. In this work, we identify the molecular basis of this selectivity for two similar systems that do not cross-talk to each other. Structural and mutational analyses reveal five key residues involved in specificity and activation mechanism, allowing us to easily manipulate ComRS toward relaxed, reverted, or new selectivity. This work is a milestone for understanding ComR-XIP coevolution and pheromone communication in streptococci.

Author contributions: L.L.-G., P.S., S.N., and P.H. designed research; L.L.-G., J.T., A.G.-E., I.E., and M.A.-N. performed research; L.L.-G., J.T., I.L.d.l.S.-G., N.L., M.A.-N., J.M., P.S., S.N., and P.H. analyzed data; and L.L.-G., J.T., J.M., P.S., S.N., and P.H. wrote the paper.

The authors declare no competing interest.

This article is a PNAS Direct Submission.

Data deposition: The atomic coordinates of apo $ComR_{Sve}$, $ComR_{Sve}$·XIP_{Sve}, and apo $ComR_{Sth}$ have been deposited in the Protein Data Bank, https://www.wwpdb.org (PDB ID codes 6HU8, 6HUA, and 6QER).

[1]L.L.-G. and J.T. contributed equally to this work.

[2]To whom correspondence may be addressed. Email: sylvie.nessler@i2bc.paris-saclay.fr or pascal.hols@uclouvain.be.

This article contains supporting information online at https://www.pnas.org/lookup/suppl/doi:10.1073/pnas.1916085117/-/DCSupplemental.

more pronounced in the peptide-binding receptor domain than in the conserved DNA-binding domain (10). Furthermore, on the basis of observed differences in XIP sequences, three general classes of ComRS systems have been proposed among the seven phylogenetic groups of the *Streptococcus* genus (10, 16). Type I peptides are characterized by the presence of a hydrophobic (V/L)P(F/Y)F motif and are exclusively found in streptococci from the salivarius group. Peptides from type II, which are found in the groups bovis, mutans, agalactiae, and pyogenes, contain a WW motif and in some cases, a basic and/or acidic residue. Because, in most *Streptococcus suis* strains, the XIP peptides do not contain two contiguous aromatic residues but display a WG(T/K)W motif, they have been classified as type III (10). A cross-talk analysis performed on ComRS systems from types II and III showed that they could be classified as strict (e.g., *Streptococcus mutans* and *S. suis*), intermediate (e.g., *Streptococcus agalactiae*) or promiscuous (e.g., *Streptococcus bovis*) based on their ability to recognize heterologous XIP peptides (24). The sequence diversity in XIP peptides and variations in ComR selectivity raise questions related to the mechanism of peptide pheromone recognition and the evolutionary driver of this divergence. Interestingly, among type I ComRS systems, cross-activation has been observed between $ComR_{Sth}$ from *Streptococcus thermophilus* LMD-9 and $ComR_{Ssa}$ from *Streptococcus salivarius* SK126, which recognize highly similar peptide sequences, i.e., XIP_{Sth} LPYFAGCL and XIP_{Ssa} LPYFTGCL, respectively (13). In turn, $ComR_{Sth}$ was not activated by the more distant type I XIP_{Sve} peptide VPFFMIYY from *Streptococcus vestibularis* F0396 (14). These two ComRS systems thus represent an interesting model to decipher the molecular basis of XIP selectivity.

Our previous structure-function analysis of the ComRS system from *S. thermophilus* LMD-9 revealed the first clues on the activation mechanism of type I ComR (25). We showed that peptide binding induces ComR dimerization and release of the HTH domain, which is sequestered in the apo form of the regulator, thus preventing inappropriate activation of competence in absence of peptide. To go further in the understanding of the molecular mechanism of peptide selectivity by ComR regulators, we present here a detailed structural and functional comparison of the ComRS systems from *S. thermophilus* and *S. vestibularis*. In particular, we solved the structure of $ComR_{Sve}$ from S. *vestibularis* F0396, alone and in complex with its cognate peptide XIP_{Sve}. We engineered ComR chimeric proteins and $ComR_{Sth}$ point mutants to perform activation assays using wild-type (WT) and hybrid peptides. Together, these results allowed us to identify residues directly involved in peptide selectivity and helped decipher the XIP-induced conformational change required for activation.

Results

Absence of Cross-Talk between $ComRS_{X1}$ and $ComRS_{X2}$. Because natural competence had not yet been demonstrated under laboratory conditions for *S. vestibularis*, and to confirm the functionality of its ComRS system, we tested its transformability in response to XIP. We showed that *S. vestibularis* F0396 is unable to be transformed in absence of its cognate XIP_{Sve} peptide but becomes competent when the pheromone is added, as observed in most strains of the salivarius group (*SI Appendix*, Table S1) (26). We then performed cross-talk experiments with a bioluminescent reporter strain of *S. thermophilus* LMD-9 (P_{comS}-*luxAB*) that is deficient for XIP production and contains a replacement of $ComR_{Sth}$ by $ComR_{Sve}$ from *S. vestibularis* F0396. The HTH DNA-binding domains of the two proteins (helices α1 to α6) display 93% sequence identity and recognize the same (pseudo)palindromic ComR box (Fig. 1). As already observed with $ComR_{Sth}$ (14), we showed that $ComR_{Sve}$ is strongly activated by addition of its cognate peptide XIP_{Sve} but not by the heterologous XIP_{Sth} (Fig. 2). This demonstrated the absence of cross-activation between these two type I ComRS systems, despite 79% sequence identity between their TPR peptide-binding domains (Fig. 1) (14).

Interaction experiments using fluorescence polarization assays demonstrated that this absence of cross-talk is directly correlated with the incapacity ($ComR_{Sve}$) or weak ability ($ComR_{Sth}$) to bind the XIP peptide of the other species (Fig. 3*A*). The data revealed that the affinity of ComR for its cognate peptide is lower in the *S. vestibularis* system compared to *S. thermophilus* with K_d values of 120.2 ± 22.5 nM and 2.0 ± 0.7 nM, respectively.

Differential scanning calorimetry (DSC) experiments showed that both ComR proteins are strongly stabilized upon binding of their cognate peptide, with a melting temperature (Tm) shifted from 35 °C to 40 °C in absence of peptide to about 75 °C in presence of peptide (Fig. 3*B*). This stabilization is most probably due to the formation of a similar dimeric complex. The thermal denaturation curve of the $ComR_{Sth}$·XIP_{Sth} complex showed a minor peak at a Tm of 35 °C, presumably reflecting an equilibrium between monomeric and dimeric forms of the protein. By contrast, the curve of the $ComR_{Sve}$·XIP_{Sve} complex displayed no peak corresponding to the monomer at a Tm of 35 °C but two small additional peaks at Tm values of 50 °C and 60 °C, revealing the formation of less stable intermediate forms. Interestingly, these two peaks disappeared in the curve obtained with the $ComR_{Sve}$·XIP_{Sve}·DNA complex, which only displayed two peaks corresponding to the stable dimer at a Tm of 75 °C and free DNA at a Tm of 65 °C (*SI Appendix*, Fig. S1*A*). We also verified that addition of DNA in the absence of peptide did not shift the Tm value of $ComR_{Sve}$ (*SI Appendix*, Fig. S1*A*).

Electrophoretic mobility shift assay (EMSA) experiments confirmed that $ComR_{Sve}$, like $ComR_{Sth}$, binds to DNA only in the presence of its cognate peptide (Fig. 3*C* and *SI Appendix*, Fig. S1*B*) and forms multimeric complexes in addition to the well-defined ComRS-DNA complex, as already observed for $ComR_{Sth}$ (25).

Together, these results demonstrate that type I ComRS systems from *S. thermophilus* and *S. vestibularis* behave similarly but are not cross-talking to each other.

Conserved XIP-Binding Mode between $ComR_{Sth}$ and $ComR_{Sve}$. To go further in the comparison of the peptide-induced activation mechanism of the two proteins, a structural analysis of $ComR_{Sve}$ was undertaken. We solved the crystal structure of the apo form of $ComR_{Sve}$ (Protein Data Bank [PDB] ID 6HU8) (27) showing that it is highly similar to apo $ComR_{Sth}$ (PDB ID 5JUF) (25), with a rmsd of 0.8 Å over 298 aligned Cα atoms. Crystal packing analysis did not identify strong intermolecular contacts, with a maximal interface area of only 789 $Å^2$ for a total surface of 15,502 $Å^2$. This confirmed that $ComR_{Sve}$ is monomeric in the absence of bound peptide as observed in solution during the purification step by size exclusion chromatography (SEC) (*SI Appendix*, Fig. S1*C*). Remarkably, the sequestrating HTH-TPR interactions observed in apo $ComR_{Sth}$ (25) are conserved in the crystal structure of apo $ComR_{Sve}$ (Fig. 4*A*).

We also solved the crystal structure of $ComR_{Sve}$ in complex with its cognate peptide XIP_{Sve} (V_1PFFMIYY$_8$). In the refined structure of the dimeric $ComR_{Sve}$·XIP_{Sve} binary complex (PDB ID 6HUA) (28), only one DNA-binding domain is visible. The second HTH domain as well as the linker region of both subunits are disordered, confirming the previous model of ComR regulation mechanism (25). This demonstrates in particular that HTH release does not require the presence of DNA and that TPR dimerization can also occur in the absence of DNA. The TPR domain of $ComR_{Sve}$·XIP_{Sve} binary complex forms a tight dimer highly similar to that observed in the ternary complex $ComR_{Sth}$·XIP_{Sth}·DNA (PDB ID 5JUB) (25), with a rmsd of 0.92 Å over 451 aligned Cα atoms (Fig. 4*B*). However, we can notice that the E282-K246 salt bridge stabilizing the $ComR_{Sth}$ dimer is replaced by a H bond between E282 and Y250 in the $ComR_{Sve}$·XIP_{Sve} complex (*SI Appendix*, Fig. S2). This may explain why less stable intermediate

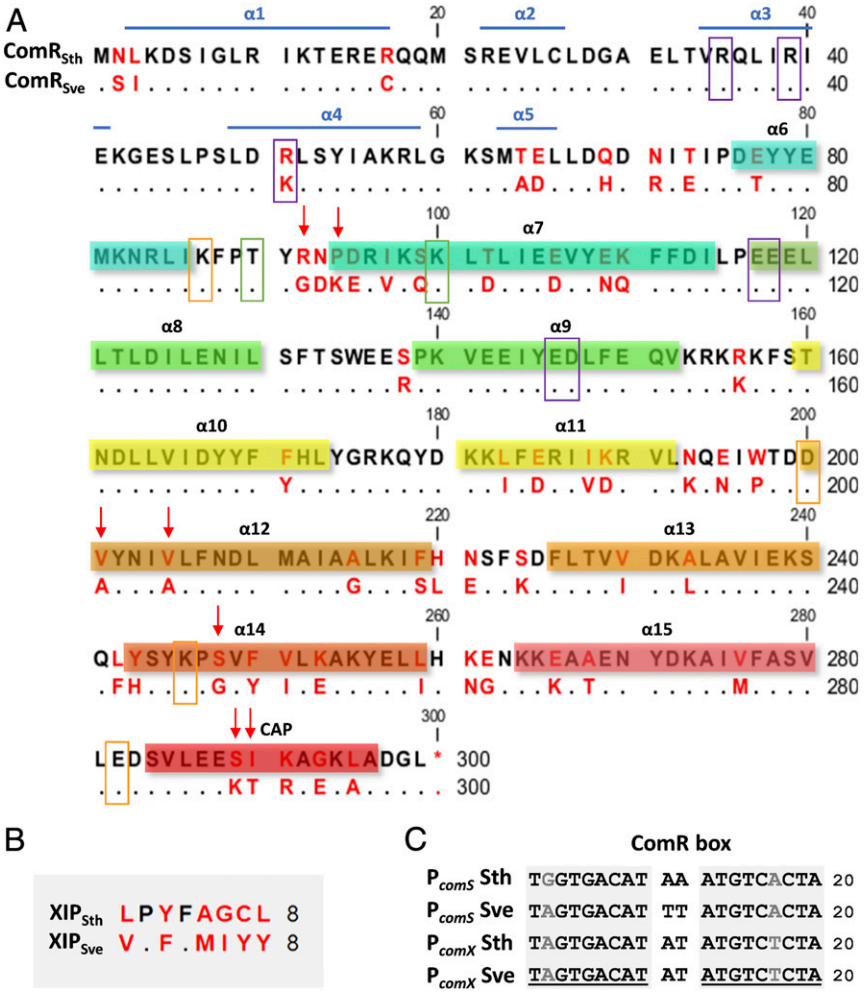

Fig. 1. Sequence alignment of ComR, XIP, and ComR box from *S. thermophilus* LMD-9 and *S. vestibularis* F0396. (*A*) ComR. The α-helices are labeled in blue in the HTH domain and colored by spectrum according to the structure representation in the TPR domain (Fig. 4). Nonconserved residues are indicated in red. Functionally important residues are highlighted: residues implicated in HTH sequestration are squared in purple (R35, R39, and R/K-51 in the HTH, and E117, E118, E146, and D147 in the TPR domain); residues involved in dimer stabilization are squared in orange (K87, D200, K246, and E282); and residues T90 and K100 interacting with the XIP C terminus are squared in green. Red arrows indicate positions of substitutions that have been introduced by mutation in ComR$_{Sth}$ (R/G-92, P/K-94, V/A-201, V/A-205, S/G-248, S/K-289, and I/T-290). (*B*) XIP. Nonconserved residues are indicated in red. (*C*) ComR box of P_{comS} and P_{comX}. The palindromic sequences are underlined. Differences in the nucleotide sequence are indicated in gray.

forms of ComR$_{Sve}$·XIP$_{Sve}$ were observed in the DSC experiments where DNA does not stabilize the dimer (Fig. 3*B* and *SI Appendix*, Fig. S1*A*).

Both ComR$_{Sve}$·XIP$_{Sve}$ and ComR$_{Sth}$·XIP$_{Sth}$·DNA complexes display a conserved peptide-binding mode despite all sequence variations (Fig. 4 *C* and *D* and *SI Appendix*, Fig. S3). The XIP octapeptide is bound with its C-terminal extremity deeply buried in the closed conformation of the pocket formed by the TPR domain while its N-terminal moiety forms a single-turn 3_{10}-helix pointing toward the solvent (Fig. 5*A*). Most polar contacts are conserved, in particular the nonspecific interaction between the peptide backbone and ComR residue N208, corresponding to the asparagine conserved in most TPR domains (29). The essential interactions between the C-terminal carboxylate of the peptide and the two residues, K100 from helix α7 and T90 from loop α6-α7 (named L6), are conserved (Fig. 4*C*) (25). XIP main chain atoms are superimposable, except for the N-terminal residue (rmsd of 0.572 Å over the eight superimposed Cα). Indeed, compared to the bound XIP$_{Sth}$, the XIP$_{Sve}$-V1 residue is rotated away from the hydrophobic pocket formed by residues F/Y-171 (aa_1/aa_2 substitution, aa_1 for Sth and aa_2 for Sve throughout the paper) and Y-174 from helix α10, thus allowing binding of residue XIP$_{Sve}$-M5 and accommodating the XIP A/M-5 substitution (Fig. 4*C*). Interestingly, the ComR R/G-92 substitution seems to be compensated by the XIP G/I-6 substitution (Fig. 4*C*). Similarly, ComR substitutions V/A-205 in helix α12 and S/G-248 in helix α14 may compensate for the XIP substitutions L/Y-8 and C/Y-7, respectively. The conservative XIP Y/F-3 substitution maintains hydrophobic interactions with the capping helix α16 (named CAP), and the impact of the ComR substitutions S/K-289, I/T-290, and G/E-293 remains unclear (Fig. 4*C*). Taken together, these observations indicate that only a few ComR substitutions may ensure peptide selectivity and prevent cross-talk between the ComRS systems from *S. thermophilus* and *S. vestibularis*.

Reversion of ComR$_{Sth}$ Selectivity by Swapping of Multiple α-Helices. In parallel to this structural analysis, a large mutagenesis program was undertaken to understand ComR-XIP specificity and validate the structural hypotheses. As a first approach, we investigated the role of the loop L6 (residues 89 to 94) and helices α7 (residues 95 to 115), α12 (residues 197 to 221), α14 (residues 242 to 262), and CAP (residues 284 to 296) in the peptide

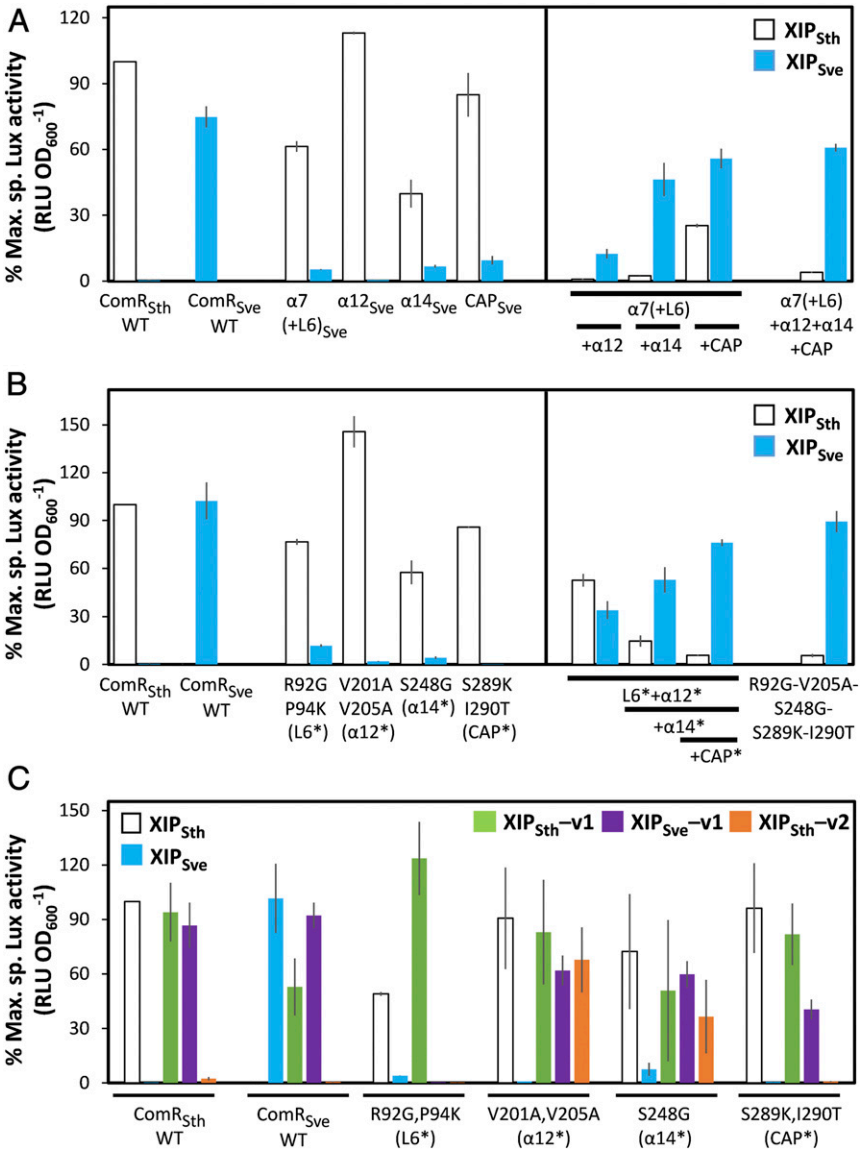

Fig. 2. In vivo selectivity assays. Maximum specific luciferase activity (RLU OD_{600}^{-1}), expressed in percentage, emitted by the *S. thermophilus* P_{comS} reporter strain. The strain producing (*A*) $ComR_{Sth}$ WT, $ComR_{Sve}$ WT, and chimeric proteins ($ComR_{Sth}$ + α-helices from $ComR_{Sve}$) grown in presence of 1 μM XIP_{Sth} (LPYFAGCL, open bars) or XIP_{Sve} (VPFFMIYY, cyan bars); (*B*) $ComR_{Sth}$ point mutants grown in presence of 1 μM XIP_{Sth} (open bars) or XIP_{Sve} (cyan bars); and (*C*) $ComR_{Sth}$ WT, $ComR_{Sve}$ WT, and $ComR_{Sth}$ point mutants grown in presence of XIP_{Sth} (open bars), XIP_{Sve} (cyan bars), XIP_{Sth}-v1 (LPYFAICL, green bars), XIP_{Sve}-v1 (VPFFM**G**YY, purple bars), or XIP_{Sth}-v2 (LPYFAG**YY**, orange bars). Bars represent the average of at least three independent repeats ± SD. Loop α6-α7 is noted L6. Point mutants are noted as L6*, α12*, α14*, and CAP*.

recognition. We engineered $ComR_{Sth}$ chimeric proteins by exchanging these TPR elements by the corresponding sequences of $ComR_{Sve}$. The transcriptional response of these chimeras to XIP_{Sth} and XIP_{Sve} peptides was then analyzed by in vivo bioluminescent assays (Fig. 2*A*). Single swapping of each individual element had only a minor impact on the activation capacity of XIP_{Sve}. Furthermore, the chimera carrying these single helix substitutions retained a complete or partial activation capacity in presence of XIP_{Sth}. By contrast, a dual substitution of α7(+L6) with either α12, α14, or CAP differentially resulted in a change of specificity. In particular, the dual swapping of α7(+L6) with α14 completely reversed the recognition strictness toward the heterologous XIP_{Sve} peptide. The same pattern was observed with the chimeric protein carrying the simultaneous substitution of the four elements, which displayed a quasisimilar behavior than $ComR_{Sve}$. Taken together, these results confirm that the TPR elements identified in the crystal structure as essential for specific XIP recognition play a major role in ComR selectivity and activation.

Reversion of $ComR_{Sth}$ Selectivity by Point Mutations. In order to gain insights into the exact roles played by substituted residues either in direct contact with the bound XIP or located in the vicinity of its binding site, we prepared several mutant proteins carrying point substitutions in the abovementioned TPR elements. The engineered $ComR_{Sth}$ mutants R92G-P94K (L6*), V205A-V201A (α12*), S248G (α14*), and S289K-I290T (CAP*) globally displayed similar XIP selectivity profiles compared to the corresponding $ComR_{Sth}$ chimeric proteins (Fig. 2*B*). Furthermore, the combination of all of these seven point mutations had the same effect as the chimeric protein carrying the simultaneous swapping of all corresponding TPR elements. Intriguingly, the tetramutant

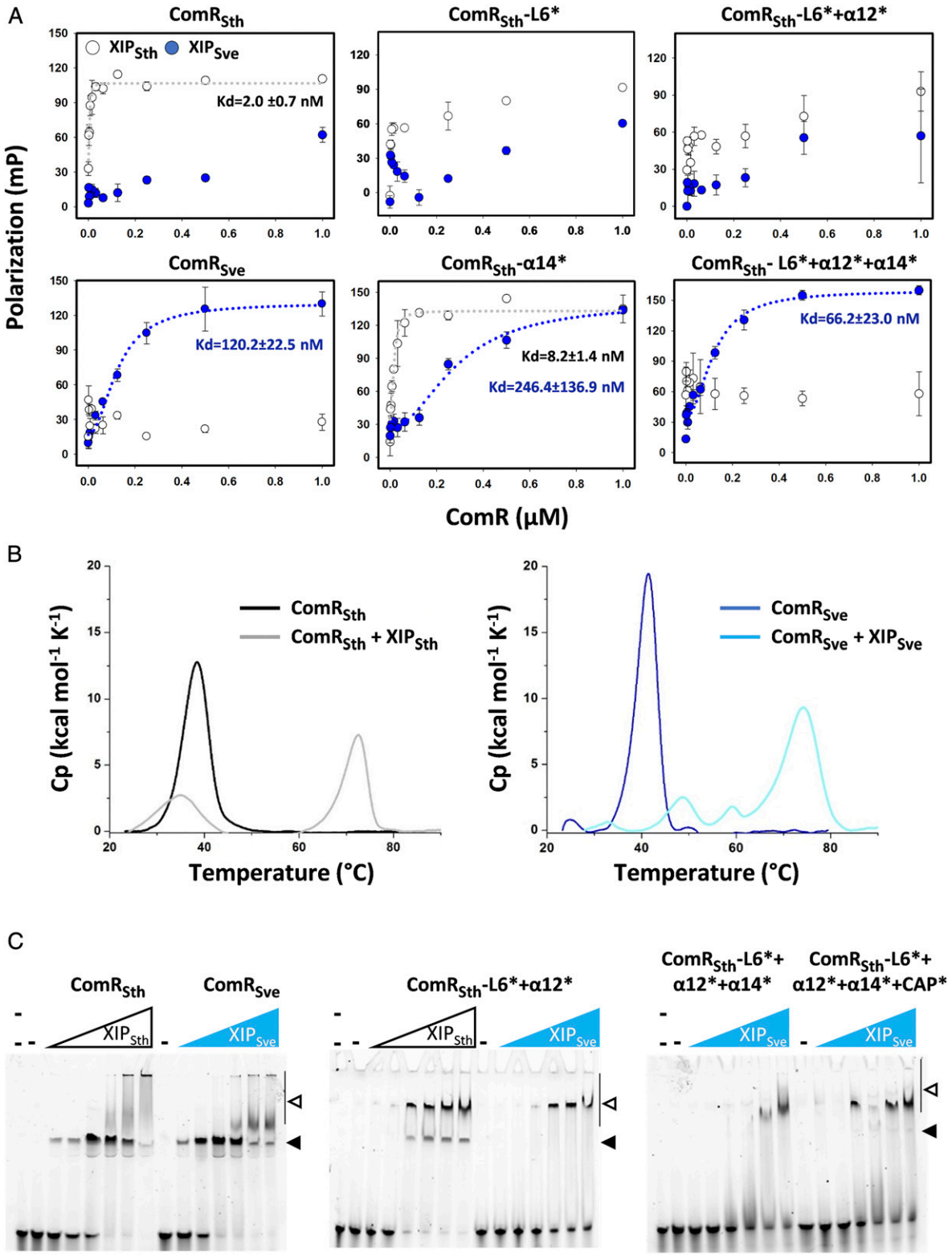

Fig. 3. In vitro interaction measurements. (*A*) Fluorescence polarization assays. Titration was performed in presence of a fixed concentration (30 nM) of FITC N-labeled XIP_{Sth} or XIP_{Sve} peptide (open or blue dots, respectively) and serial dilutions of ComR starting from 1 μM. Experimental values represent the averages ± SD of at least three replicates. Curves reaching the saturation were fitted by the one ligand-binding site equation to deduce the apparent K_d value. (*B*) DSC analysis of ComRs WT. Comparison of the variation of heat capacity (Cp) during thermal denaturation of 15 μM ComR alone and in complex with 150 μM of the cognate XIP peptide. The thermal transition midpoint (Tm) representing the stability of the sample was determined from the top of the DSC peak. We verified that the peptide alone did not give any signal. (*C*) EMSA. Labeled P_{coms} 40-bp DNA fragments (20 ng) were incubated with a fixed concentration of ComRs WT or mutants (1 μM, except for $ComR_{Sth}$-L6*+α12* used at 4 μM) in absence of peptide (–) or in presence of increasing concentrations of peptide (from 0 to 2 μM, except for $ComR_{Sth}$-L6*+α12*, which was incubated with 0 to 8 μM XIP). The well-defined ComR-XIP-DNA complex and multimeric complexes are respectively indicated by closed and open arrowheads. One representative experiment of at least two independent replicates is shown.

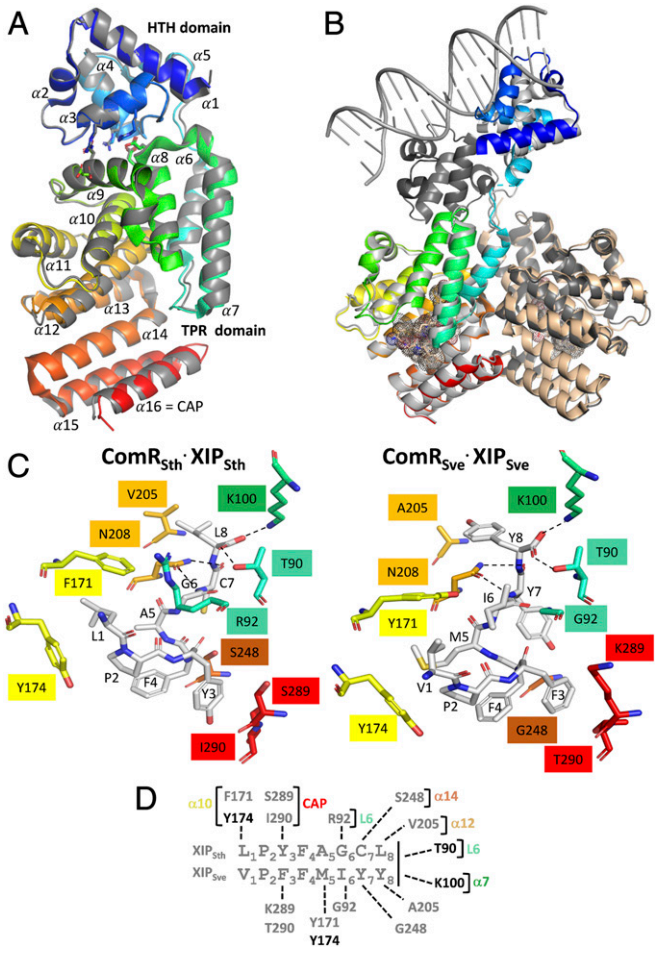

Fig. 4. Structural comparison of $ComR_{Sth}$ and $ComR_{Sve}$. (*A*) Superimposition of the apo forms. The superimposed crystal structures of the proteins are shown as cartoon. $ComR_{Sve}$ (PDB ID 6HU8) (27) is colored by spectrum from blue (N-ter) to red (C-ter). $ComR_{Sth}$ (PDB ID 5JUF) (25) is shown in gray. The α-helices are labeled as well as the HTH and TPR domains. (*B*) Superimposition of the $ComR_{Sve}$·XIP_{Sve} and $ComR_{Sth}$·XIP_{Sth}·DNA complexes. The proteins are shown in cartoon representations and the bound peptides are shown in sticks and highlighted by dots. The ternary complex from *S. thermophilus* (PDB ID 5JUB) (25) is colored in gray. One subunit of the binary complex from *S. vestibularis* (PDB ID 6HUA) (28) is colored by spectrum and the second subunit, whose HTH domain is not visible, is shown in beige. (*C*) Residues involved in peptide binding. The bound peptides are shown in sticks, colored by atom types, and their residues are labeled. Most relevant ComR residues are highlighted in sticks, colored by spectrum as the α-helices in *A* and *B*. Their labels are colored accordingly. (*D*) Summary of ComR-XIP interactions. Identical and different ComR residues interacting with peptides are in black and gray, respectively.

combining R92G-P94K and V201A-V205A (L6*+α12*) has dual specificity, contrasting with the corresponding helix-swapped chimera that is not activated by XIP_{Sth}. This suggests that an additional substitution(s) in α12 is required to restore the strict profile observed with the complete exchange of helix α12. However, increased selectivity toward XIP_{Sve} was partially restored upon addition of the fifth α14* mutation S248G compensating the C/Y-7 XIP substitution, and fully recovered upon further addition of the CAP* mutations S289K-I290T, which shows that they play a major role in the recruitment of the CAP helix by the XIP_{Sve} residue F3. In addition, we verified using EMSA experiments that the multiple mutants of $ComR_{Sth}$, which are activated by XIP_{Sve}, can bind DNA in presence of this heterologous peptide (Fig. 3*C* and *SI Appendix*, Fig. S1*B*). By careful examination of the structure, residues 94 and 201 were identified as less essential in the protein-peptide interaction. Indeed, reversion of these two mutations had no impact on the inversion of peptide selectivity. Hence, we showed that a $ComR_{Sth}$ mutant protein carrying only five substitutions (i.e., R92G-V205A-S248G-S289K-I290T) displayed a full inversion of peptide selectivity (Fig. 2*B*). This emphasizes the fact that stabilization of the active closed conformation of the TPR domain requires not only the recruitment of loop L6 through interactions between residues XIP-6 and ComR-92 but also recruitment of CAP through interactions of the peptide with helices α12 and α14.

Tight Interconnection between XIP Affinity and Activation Effect. In order to compare the involvement of the abovementioned residues in in vitro peptide binding with in vivo transcriptional activation, the affinity of $ComR_{Sth}$ point mutants for XIP_{Sth} and XIP_{Sve} was measured by fluorescence polarization (Fig. 3*A*). Comparison with the fluorescence data obtained with the WT protein demonstrated that the R92G-P94K (L6*) mutations alone decreased the affinity of $ComR_{Sth}$ for its cognate peptide and slightly improved the interaction with XIP_{Sve}, whereas V205A-V201A (α12*) or S289K-I290T (CAP*) mutations did not significantly affect the peptide affinity of $ComR_{Sth}$ (*SI Appendix*, Fig. S1*D*). Combination of L6* and α12* mutations produced a promiscuous receptor with similar and low affinity for both peptides, mainly due to L6* mutations. Surprisingly, the S248G (α14*) mutation showed an essential role for XIP_{Sve} binding, with an estimated K_d value of 246.4 ± 136.9 nM, similar to the K_d of the natural receptor $ComR_{Sve}$ (120.2 ± 22.5 nM). This result contrasts with the absence of in vivo activation observed with the α14* mutation in presence of XIP_{Sve} (Fig. 2*B*), which could be explained by a lack of activating conformational change even if the pocket of this mutant protein accommodates the noncognate peptide. Interestingly, the α14* mutation only weakly affected the affinity for XIP_{Sth} (K_d = 8.2 ± 1.4 nM) and required its combination with L6* and α12* mutations to achieve inversion of selectivity, with a K_d value of 66.2 ± 23.0 nM for XIP_{Sve}. Further addition of the CAP* mutations had almost no effect on the affinity for XIP_{Sve} (K_d value of 70.3 ± 42.4 nM) (*SI Appendix*, Fig. S1*D*), suggesting that they do not play an essential role in peptide binding but might be important for the stabilization of the closed conformation of the TPR domain. These results nicely correlate with the in vivo activity assays (Fig. 2 *A* and *B*) and further emphasize the role of the R/G-92 and S/G-248 ComR substitutions compensating the G/I-6 and C/Y-7 XIP substitutions. Taken together, they show that affinity and activating effect of the peptide are tightly interconnected with selectivity.

Compensating Mutations between XIP and ComR. In order to validate the essential role played by the abovementioned compensating substitutions, we evaluated the impact of various XIP variants on ComR selectivity. In a first step, we investigated the compensating substitution XIP G/I-6 versus ComR R/G-92. For this purpose, we tested the activity of the hybrid variants XIP_{Sth}-v1 (LPYFA**I**CL) and XIP_{Sve}-v1 (VPFFM**G**YY) on both WT proteins and on the $ComR_{Sth}$ point mutants (Fig. 2*C*), as well as the chimera with swapped helices (*SI Appendix*, Fig. S4*A*). Notably, both WT proteins $ComR_{Sth}$ and $ComR_{Sve}$ were efficiently activated by these two XIP variants, showing that a single XIP substitution at position 6 could result in cross-activating peptides. In particular, whereas XIP_{Sve} was totally inefficient with $ComR_{Sth}$, introducing a G residue at position 6 is sufficient for proper binding of the peptide variant XIP_{Sve}-v1 (VPFFM**G**YY) and stabilization of the active closed conformation of the protein. However, activation of $ComR_{Sth}$ by XIP_{Sth}-v1 (LPYFA**I**CL) demonstrates that the I6 residue impairing the binding of XIP_{Sve} does not have the same effect when introduced in XIP_{Sth}. This

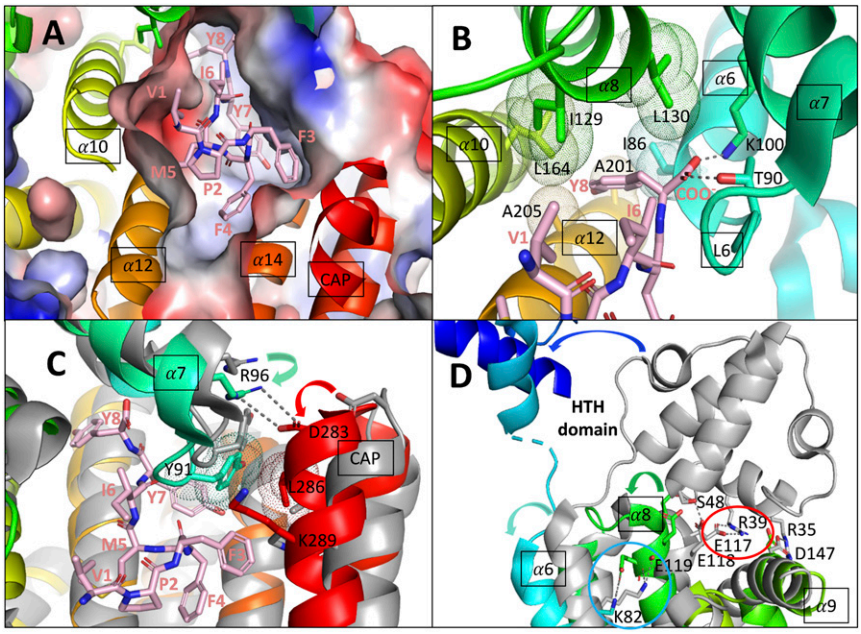

Fig. 5. Structural insights into ComR activation mechanism. The protein from the $ComR_{Sve}$·XIP_{Sve} binary complex (PDB ID 6HUA) (28) is represented as cartoon and colored by spectrum as in Fig. 4. Loop L6 and important helices are labeled. The bound XIP_{Sve} (VPFFMIYY) is represented in sticks as in Fig. 4*C*. (*A*) XIP-binding pocket. The closed peptide-bound pocket of $ComR_{Sth}$ is shown as surface colored by electrostatic potential (basic regions in blue, acidic region in red, and nonpolar residues in white). (*B*) Recruitment of loop L6. Residues from helices α6, α8, α10, and α12 forming the hydrophobic pocket where residue XIP_{Sve}-Y8 binds are shown in sticks and dots. The interactions between the C-terminal carboxylate (COO^-) group of the peptide and residues K100 and T90 are shown as black dashed lines. (*C*) Stabilization of the TPR closed conformation. The complex $ComR_{Sve}$·XIP_{Sve} is superimposed with the apo form of $ComR_{Sve}$ (PDB ID 6HU8) (27) shown as cartoon colored in gray. The shifts of helices α7 and CAP are highlighted by green and red arrows, respectively. The stabilizing salt bridge between R96 and D283 is shown as black dashed lines. Residues Y91 and L286 forming a hydrophobic stacking interaction are shown as sticks and dots. (*D*) Release of the HTH domain. The superimposed structures of the apo and peptide-bound forms of $ComR_{Sve}$ are colored as in *C*, shown from the opposite face compared to *A*–*C*. The shift of α6 (cyan arrow) is transmitted to α8 (green arrow) through the conserved salt bridge between residues K82 and E119 (red circle). The resulting break of the salt bridge between E117 and residue R39 from helix α3 (blue circle) releases the HTH domain, which is shifted away (blue arrow).

suggests that the steric clash between XIP_{Sve}-I6 and $ComR_{Sth}$-R92 that was expected from the structure analysis (Fig. 4*C*) can be avoided in the context of the XIP_{Sth} sequence. Reciprocally, the requirement of XIP-I6 for $ComR_{Sve}$ activation is only needed in the XIP_{Sth} context, further emphasizing the complexity of the peptide recognition mechanism. Finally, the $ComR_{Sth}$ R92G-P94K (L6*) mutant was efficiently activated by the XIP_{Sth}-v1 (LPYFA**I**CL) containing the compensating XIP G/I-6 substitution but was only poorly or not activated by the peptides containing a G residue at position 6, i.e., XIP_{Sth} (LPYFAGCL) and XIP_{Sve}-v1 (VPFFM**G**YY). Moreover, the swap of helix α7(+L6) had a dominant-negative effect on XIP_{Sve}-v1 activation when combined with swapped α12, α14, or CAP, reinforcing the importance of this complementarity for activation (*SI Appendix*, Fig. S4*A*).

Together, these results thus confirm the importance of the compensation between XIP G/I-6 and ComR R/G-92 for activation. They also support the key role of residue XIP-6 in controlling the selectivity of peptide recognition.

In a second step, we addressed the importance of compensating substitutions XIP L/Y-8 and C/Y-7 versus ComR V/A-205 and S/G-248 in peptide selectivity by introducing the double substitution L/Y-8 and C/Y-7 in XIP_{Sth} (XIP_{Sth}-v2 LPYFAG**YY**), which is characteristic of the C terminus of XIP_{Sve} (Fig. 2*C*). The modified peptide XIP_{Sth}-v2 impaired activation of both $ComR_{Sth}$ and $ComR_{Sve}$. However, activation of $ComR_{Sth}$ by XIP_{Sth}-v2 was partially restored by the mutations V201A-V205A (α12*) or S248G (α14*), supporting the complementarity between compensating substitutions. Intriguingly, both WT ComR are activated by XIP_{Sve}-v1 (VPFFM**G**YY) but not by XIP_{Sth}-v2 (LPYFAG**YY**), suggesting that interactions involving the N terminus of the bound peptide (i.e., residues LPYFA versus VPFFM) could also play an important role in the activating conformational change.

DSC experiments (*SI Appendix*, Fig. S4*B*) showed that binding of XIP_{Sth}-v1 had the same stabilizing effect as the WT peptide on $ComR_{Sth}$ but only resulted in intermediate forms of the complex with $ComR_{Sve}$. In turn, neither of the two proteins was shifted to the highly stable form upon binding of XIP_{Sve}-v1, which only resulted in less stable complexes. Finally, the scans obtained in presence of the inactive XIP_{Sth}-v2 variant were highly similar to the apo form of $ComR_{Sth}$ and $ComR_{Sve}$. Interestingly, EMSA experiments demonstrated that the less stable complexes formed by $ComR_{Sth}$ and $ComR_{Sve}$ with either XIP_{Sth}-v1 or XIP_{Sve}-v1 shifted DNA in a similar manner than the cognate complexes (*SI Appendix*, Fig. S4*C*). These results thus demonstrate that noncognate peptides can bind to ComR regulators and form alternative active complexes.

Finally, we can conclude that these results allowed us to identify key XIP and ComR residues directly implicated in the activating conformational change and the main compensatory substitutions that lead to divergence in peptide selectivity between the two type I ComRS systems.

Integrative View between ComR Selectivity and Activation. Resolution of a new crystal structure of $ComR_{Sth}$ apo form (PDB ID 6QER) (30) demonstrated that the superhelix of the peptide-free TPR domain can adopt distinct conformations (*SI Appendix*, Fig. S5 *A* and *B*), thus demonstrating the structural plasticity of the monomeric open conformation of ComR. Modeling analysis showed that, in both $ComR_{Sve}$ and $ComR_{Sth}$ proteins, the closed conformation of the peptide-binding pocket, which is not accessible to the peptide from outside of the protein (Fig. 5*A*), can however easily accommodate all noncognate (active and inactive)

XIP peptides used in this study. In particular, a simple shift of the R92 side chain allows modeling of XIP_{Sve} in the pocket of $ComR_{Sth}$ without any clash with XIP-I6 (*SI Appendix*, Fig. S6). Together, these results suggest that the pheromone first binds in the flexible open conformation of the TPR pocket and that the activation mechanism mostly relies on the ability of the peptide to stabilize the closed conformation of the TPR domain.

At the bottom of the open pocket, helices α14 and α12 most probably form the first binding scaffold for the peptide (Fig. 4*C*). This would explain the essential role in peptide selectivity played by residues 205 (from α12) and 248 (from α14), which accommodate the XIP substitutions L/Y-8 and C/Y-7, respectively. Formation of an essential salt bridge between the C-terminal carboxyl group of the peptide and the conserved α7 residue K100 (25) ensures the recruitment of loop L6 via an additional H bond with residue T90 from the conserved $P_{89}T_{90}Y_{91}$ motif. Proper positioning of the carboxylate requires the binding of residue XIP-8 in the hydrophobic pocket formed by residues from helices α6, α8, α10, and α12 (Figs. 4*C* and 5*B*). Our mutational analysis further highlighted the essential role played by the compensating XIP G/I-6 and ComR R/G-92 substitutions in loop L6 recruitment and peptide selectivity. Comparison of the structures showed that, in both ComRS systems, the recruitment of loop L6 results in a small shift of helix α7, and in particular of its conserved residues Y91 and R96 (Fig. 5*C*). At the other end of the TPR domain, the CAP helix is recruited by a hydrophobic interaction between residues 289 to 290 and XIP-3 and shifted toward α7, allowing the formation of 1) a salt bridge between residues R96 and D283 and 2) a hydrophobic stacking interaction between Y91 and L286, thus ensuring stabilization of the closed conformation (Fig. 5*C*). These movements further allow stabilization of the TPR dimer, in particular through reorientation of the conserved residue E282 from the loop preceding the CAP helix, which is directly involved in the interaction with the neighboring subunit (*SI Appendix*, Fig. S2). In addition, they also result in the release of the sequestered HTH domains. In particular, we observed in both ComRS systems that the recruitment of loop L6 is associated with a shift of helix α6. The latter contains residue K82, which forms a conserved salt bridge with E119 from α8 in the absence of bound peptide (Fig. 5*D*). This strong interaction allows proper positioning of α8 and formation of the sequestering interaction between E117 and R39 from helix α3 (25). Upon peptide binding, the break of the K82-E119 interaction might play an essential role in the disruption of the interaction between HTH and TPR domains.

The proposed mechanism thus explains how peptide binding induces the break of helix α9 shown to be essential for the release of the sequestered HTH domain and the dimerization required for DNA binding.

Discussion

This structural and functional comparison between two type I ComRS systems that do not cross-talk to each other sheds light on the molecular determinants responsible of pheromone selectivity. In addition, modified sensors and pheromones were generated that allowed communication between these two signaling systems due to either high promiscuity or exchange in specificity. This work also highlighted the role of key residues in ComR-XIP complementarity and helped gain a better understanding of the peptide-induced activation mechanism of ComRS systems.

Two crystal structures of $ComR_{Sve}$ were solved in this study, its apo form and the binary complex with XIP_{Sve}. They demonstrate that the overall activation mechanism, initially proposed for the protein from *S. thermophilus* (25), is conserved in *S. vestibularis* (Fig. 6). In particular, we confirmed our previous hypothesis suggesting that, in the absence of bound DNA, the ComR·XIP complex dimerizes while the sequestered HTH domains are released and freely float around the TPR dimer through highly flexible linkers. Comparison of the $ComR_{Sve}$·XIP_{Sve} binary complex with the previously published ternary complex $ComR_{Sth}$·XIP_{Sth}·DNA (25), together with an extensive mutagenesis analysis based on the transfer of $ComR_{Sve}$ features in $ComR_{Sth}$ mutants, allowed us to unravel the atomic details of the peptide-induced activation mechanism of type I ComR regulators (Fig. 5). This mechanism relies on an initial pheromone selection by the TPR domain in an open conformation, in which helix α14 plays a predominant role for peptide discrimination. Then, we proposed that the recruitment of the first TPR motif (α6-L6-α7) by the C terminus of the XIP peptide acts as a "toggle switch" for the conformational change of the whole TPR domain from an open to a closed conformation (Fig. 6). We suggest that this shift allows 1) the stabilization of the CAP helix (via α7-CAP and XIP-CAP interactions) in a configuration that induces dimerization and 2) the reorientation of key

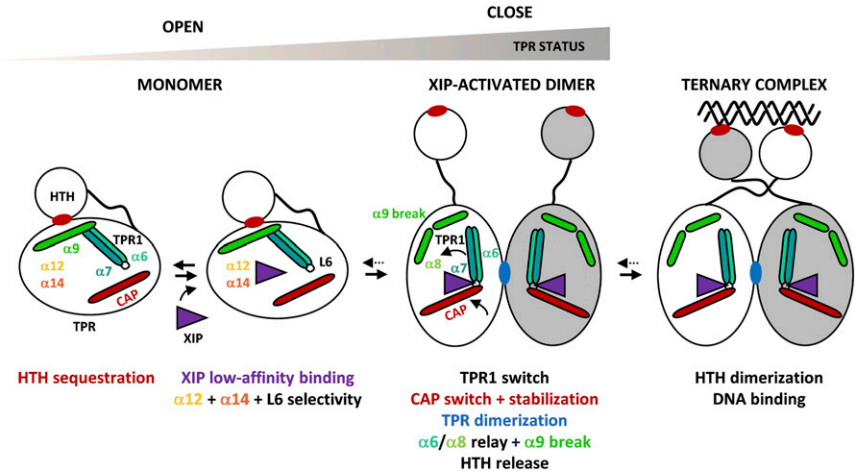

Fig. 6. Schematic drawing of the proposed XIP-driven activation mechanism of ComR. The HTH and TPR domains of the protein are shown with the flexible linker. Helices α12, α14, and L6 implicated in peptide binding are labeled. Helices α6, α7, α8, α9, and CAP, which are directly implicated in the activating conformational change, are shown as sticks and labeled. Helices are colored as in Fig. 4. Red and blue ellipses represent residues involved in HTH sequestration and TPR dimerization, respectively. While dimeric binary and ternary complexes have been shown experimentally, the monomeric ComR-XIP low-affinity complex remains hypothetical.

residues resulting in HTH release (via an α6-α8 relay and a break of α9) (Fig. 6). This highly detailed structure-function analysis thus allows us to gain a deep understanding of ComR selectivity.

The crystal structure of type III $ComR_{Ssu}$ from *S. suis* (PDB ID 5FD4) (24) displayed the same overall apo conformation characterized by the HTH sequestration, suggesting that a similar mechanism occurs in all ComR regulators. A modeling and mutagenesis analysis performed on type II and type III ComR proteins by using this structure of apo $ComR_{Ssu}$ as a guide suggested that a conserved face of the peptide-binding pocket could contribute to XIP binding, whereas a more variable face could be involved in pheromone selectivity (24).

Here, we demonstrated that five amino acid substitutions are mainly responsible for the distinct peptide specificity of the two closely related type I XIP sensors. In particular, we showed that the conversion of $ComR_{Sth}$ is associated with progressive trade-offs between initial and new function, whereas intermediate mutants (e.g., L6*+α12*) can be described as generalist receptors that are responsive to both XIPs (Fig. 2*B*). In addition, we also demonstrated that a single mutation at position 6 in either of the two XIP sequences induced cross-talk between these two cell-to-cell communication systems (Fig. 2*C*). These results show that XIP can easily evolve from a strict pheromone toward a promiscuous-inducing peptide for type I ComR sensors. Reciprocally, we also generated the XIP_{Sth}-v2 variant (LPYFAG**YY**), which cannot activate WT $ComR_{Sth}$ and $ComR_{Sve}$, but instead activates the $ComR_{Sth}$ mutants α12* and α14* (Fig. 2*C*), therefore highlighting that the mutated residues compensate the XIP C/Y-7 and L/Y-8 substitutions.

In nature, a progressive coevolution of the pheromone/receptor couple should be the real scenario and it is not clear whether the evolutionary trajectory would involve more or less generalist systems. However, such generalist receptors were previously reported for type II ComRS systems of the bovis group of streptococci (24). Although the advantages of highly selective versus promiscuous ComRS systems in complex microbial populations are not clearly understood yet (24), our results indicate that the ComRS system is easily evolvable into each direction. The receptor and pheromone alleles might coevolve sequentially in an "evolutionary ratchet," dictated either by a mutation in XIP or ComR. Based on our results showing fast XIP evolvability, one possible scenario would be an initial single mutation in the XIP sequence. This modification in the signaling peptide may slightly reduce its activation capacity (e.g., XIP_{Sth}-v1 and XIP_{Sve}-v1), and be followed by the selection of modifications in the receptor in order to optimize protein interactions (e.g., XIP-6 and ComR-92 positions). It is interesting to note that sequence alignment of type I ComR proteins revealed a higher mutation rate in α-helices that are in close contact with the XIP peptide (i.e., α7[+L6], α14, and CAP) (*SI Appendix*, Fig. S7) as well as a strong conservation of the substituted residues involved in XIP selectivity (*SI Appendix*, Figs. S7 and S8). Moreover, in addition to the previously reported type I XIPs, i.e., LPYF[A/T]GCL and VPFFMIYY, a deeper investigation of type I ComRS systems revealed the presence of three additional XIP variants (i.e., APFFIIYY, APFFINYY, and CPVLIHYL) (*SI Appendix*, Fig. S8). As found in $ComR_{Sve}$, their corresponding ComR proteins contained G92 to accommodate a XIP bulky residue (I, N, or H) at position 6. The most divergent XIP peptide CPVLIHYL showed a remarkable conservation of ComR residues involved in selectivity (i.e., XIP-H6/ComR-G92, Y7/G248, L8/V208) as well as a lack of conservation for ComR S/K289 and I/T290 corroborating the absence of a XIP aromatic residue at position 3 (*SI Appendix*, Fig. S8). These in silico observations strengthen the coevolution scenario as well as the identification of the key residues involved in selectivity.

Finally, the dissection of the molecular regulatory mechanism of ComR and understanding of the structural determinants of its peptide pheromone selectivity exposed here also paves the way toward the rational design and/or directed evolution of artificial transcriptional control and chemical communication based on ComRS systems with a large potential of applications in the fields of synthetic biology and pathogen biocontrol (e.g., quorum enhancers/quenchers).

Materials and Methods

Bacterial Strains, Plasmids, Oligonucleotides, and Growth Conditions. See *SI Appendix, Materials and Methods*. Bacterial strains, plasmids, and oligonucleotides used in this study are listed in *SI Appendix*, Tables S2–S4.

Transformation Assays, DNA Techniques, Genetic Constructions, Protein Purification, and In Silico Analyses. See *SI Appendix, Materials and Methods*.

XIP Peptide Preparation. Synthetic XIP octapeptides and fluorescein isothiocyanate (FITC) N-labeled nonapeptides were supplied by Peptide 2.0 or GeneScript and resuspended in 100% dimethyl sulfoxide (DMSO) (vol/vol).

Luciferase Assays. Luciferase assays were performed as previously described (14). Growth (OD_{600}) and luciferase (Lux) activity (expressed in relative light units [RLUs]) of the cultures were monitored after addition of synthetic XIP peptide (1 μM) during 24 h in a multiwell plate reader (Hidex Sense, Hidex).

Electrophoretic Mobility Shift Assays. A fixed concentration of purified ComR protein was mixed with a 40-bp dsDNA fragment (20 ng) carrying the ComR box of P_{coms} coupled to the Cy3 fluorophore in absence or presence of increasing amounts of XIP peptide as previously described (14). $ComR_{Sth}$-L6*+α12*+α14* (1 μM) and $ComR_{Sth}$-L6*+α12*+α14*+CAP* (1 μM) were mixed with twofold serial dilutions of XIP at an initial concentration of 2 μM. $ComR_{Sth}$-L6*+α12* (4 μM) was mixed with twofold serial dilutions of XIP at an initial concentration of 8 μM. Increased concentrations of $ComR_{Sth}$-L6*+α12* and XIP were used to better visualize the complexes as this mutant has a lower affinity for both WT XIPs. $ComR_{Sth}$·XIP_{Sth} and $ComR_{Sve}$·XIP_{Sve} WT controls were respectively assayed in the two above-cited conditions. Negative controls were performed with 1 μM ComR in absence or presence of 2 μM XIP. Peptide variants were tested at a fixed concentration of 1 μM ComR WT. The samples (20 μL) prepared in binding buffer (20 mM Tris·HCl, pH 8.0, 150 mM NaCl, 1 mM ethylenediaminetetraacetic acid (EDTA), 10% glycerol [vol/vol], 1 mg·mL^{-1} BSA) were incubated at 37 °C for 10 min prior to analysis on a native 4 to 20% gradient gel (iD PAGE gel; Eurogentec) in Tris-MOPS buffer (50 mM Tris-base, 50 mM 3-(*N*-morpholino)propanesulfonic acid, 1 mM EDTA, pH 7.7). DNA complexes were detected by fluorescence on the Ettan DIGE Imager with bandpass excitation and emission filters of 540/25 and 595/25 nm, respectively (GE Healthcare).

Fluorescence Polarization Assays. Increasing concentrations of purified ComR were mixed with a FITC N-labeled version (9 aa) of XIP_{Sth} or XIP_{Sve} peptides (ILPYFAGCL and AVPFFMIYY, respectively) at a fixed concentration of 30 nM. The samples were prepared in a final volume of 100 μL in binding buffer (20 mM Tris·HCl, pH 7.5, 150 mM NaCl, 1 mM EDTA, 10% glycerol [vol/vol]) and incubated for 10 min at 30 °C in black well 96-well plates (Greiner). Anisotropic measurements were performed in a multiwell plate reader (Hidex Sense, Hidex) in polarization mode with 485/10-nm and 535/20-nm excitation and emission filters, respectively. In order to calculate K_d values, curves that reached saturation were fitted by the one ligand-binding site equation using the SigmaPlot software.

Differential Scanning Calorimetry. Purified ComR samples (15 μM) were analyzed alone and in presence of XIP peptides (150 μM) in the protein SEC buffer in presence of 2% DMSO (vol/vol) by using a MicroCal PEAQ-DSC Automated system (Malvern). Samples of 350 μL were heated from 20 °C to 90 °C using a 1 °C/min rate. The thermal behavior of samples was recorded and analyzed using the MicroCal PEAQ-DSC software and the thermal transition midpoint (Tm) representing the stability of the sample was determined at to the top of the DSC peak. The effect of DNA was tested by addition of a 20-bp dsDNA fragment carrying the ComR box of P_{comX} (45 μM). We also verified that the peptide alone did not give any signal.

Crystal Structure Determination. Crystallization trials were performed at 18 °C using a Cartesian robot and commercial kits. Initial hits were reproduced and optimized manually using the hanging drop method and homemade solutions. The apo form of $ComR_{Sve}$ crystallized at a concentration of 20 mg·mL^{-1} in 20% polyethylene glycol (PEG) 3350 (wt/vol), 150 mM DL-malic acid, pH 7.0. The complex $ComR_{Sve}$·XIP_{Sve} crystallized in 12% PEG 4000 (wt/vol), 100 mM

$MgCl_2$, 100 mM NaCl, 100 mM trisodium citrate, pH 5.5, at a protein concentration of 6.6 mg·mL^{-1} in presence of 1.5 mM peptide. Crystals were flash frozen in the crystallization solution supplemented with 25 to 30% glycerol (vol/vol) and conserved in liquid nitrogen prior to X-ray diffraction assays.

Diffraction data were collected at the French synchrotron SOLEIL on beamline Proxima-2 for the apo form of $ComR_{Sve}$ and on beamline Proxima-1 for the $ComR_{Sve}$·XIP_{Sve} complex. The crystals diffracted at 1.9-Å and 3.4-Å resolution, respectively. The data were processed using XDS (31) and the initial phases were determined by molecular replacement using PHASER (32). The structure of apo $ComR_{Sth}$ (PDB ID 5JUF) (25) and the TPR domain from the $ComR_{Sth}$·XIP_{Sth}·DNA crystal structure (PDB ID 5JUB) (25) were used as initial models for the apo form of $ComR_{Sve}$ and its complex with XIP_{Sve}, respectively. The resulting models of $ComR_{Sve}$ (PDB ID 6HU8) (27) and $ComR_{Sve}$·XIP_{Sve} (PDB ID 6HUA) (28) were refined using PHENIX Wizard (33) and manually optimized using COOT (34). The statistics of the diffraction datasets and of the refined models are given in *SI Appendix*, Table S5.

Crystal packing analysis and structure comparison were performed using PISA (35) and PDBeFold (36), respectively. Peptide-protein interactions were analyzed and illustrated by LIGPLOT+ (37). The figures were prepared by using the PyMOL Molecular Graphics System, Version 2.0 Schrödinger, LLC.

Data Availability. The atomic coordinates of apo $ComR_{Sver}$, $ComR_{Sve}$·XIP_{Sver}, and apo $ComR_{Sth}$ have been deposited in the Protein Data Bank, https://www.rcsb.org (PDB ID codes 6HU8, 6HUA, and 6QER, respectively). All data and protocols reported are contained in the manuscript and *SI Appendix*.

ACKNOWLEDGMENTS. The crystallization assays and the calorimetry experiments were performed on the IBiSA (Biology Health and Agronomy Infrastructures)-labeled platforms from the Institute for Integrative Biology of the Cell (I2BC) (https://www.i2bc.paris-saclay.fr/spip.php?article281&lang=fr), supported by the French Infrastructure for Integrated Structural Biology ANR-10-INBS-05. The X-ray diffraction experiments were performed on beamlines Proxima-1 and Proxima-2 at SOLEIL Synchrotron, France, as well as on beamlines ID30b, ID29, and ID23 at the European Synchrotron Radiation Facility, Grenoble, France. We are grateful to the local contacts at both sites for providing assistance as well as to their synchrotron staff for smoothly running the facility. Funding: This work was supported by the Belgian National Fund for Scientific Research (FNRS), the Interuniversity Attraction Poles Programme of the Belgian Science Policy Office, and the Concerted Research Actions from Federation Wallonia-Brussels. J.T. was supported by a PhD fellowship from the French Ministère de l'Enseignement Supérieur, de la Recherche et de l'Innovation. P.H. is Senior Research Associate at FNRS.

1. F. Griffith, The significance of pneumococcal types. *J. Hyg. (Lond.)* **27**, 113–159 (1928).
2. C. Johnston, B. Martin, G. Fichant, P. Polard, J. P. Claverys, Bacterial transformation: Distribution, shared mechanisms and divergent control. *Nat. Rev. Microbiol.* **12**, 181–196 (2014).
3. M. Blokesch, Natural competence for transformation. *Curr. Biol.* **26**, R1126–R1130 (2016).
4. M. G. Lorenz, W. Wackernagel, Bacterial gene transfer by natural genetic transformation in the environment. *Microbiol. Rev.* **58**, 563–602 (1994).
5. S. M. Lattar *et al*., A Mechanism of unidirectional transformation, leading to antibiotic resistance, occurs within nasopharyngeal pneumococcal biofilm consortia. *MBio* **9**, e00561-18 (2018).
6. J. P. Claverys, M. Prudhomme, I. Mortier-Barrière, B. Martin, Adaptation to the environment: *Streptococcus pneumoniae*, a paradigm for recombination-mediated genetic plasticity? *Mol. Microbiol.* **35**, 251–259 (2000).
7. J. Lin, L. Zhu, G. W. Lau, Disentangling competence for genetic transformation and virulence in *Streptococcus pneumoniae*. *Curr. Genet.* **62**, 97–103 (2016).
8. M. Carrolo, F. R. Pinto, J. Melo-Cristino, M. Ramirez, Pherotype influences biofilm growth and recombination in *Streptococcus pneumoniae*. *PLoS One* **9**, e92138 (2014).
9. W. Y. Wholey, T. J. Kochan, D. N. Storck, S. Dawid, Coordinated bacteriocin expression and competence in *Streptococcus pneumoniae* contributes to genetic adaptation through neighbor predation. *PLoS Pathog.* **12**, e1005413 (2016).
10. L. Fontaine, A. Wahl, M. Fléchard, J. Mignolet, P. Hols, Regulation of competence for natural transformation in streptococci. *Infect. Genet. Evol.* **33**, 343–360 (2015).
11. L. S. Håvarstein, G. Coomaraswamy, D. A. Morrison, An unmodified heptadecapeptide pheromone induces competence for genetic transformation in *Streptococcus pneumoniae*. *Proc. Natl. Acad. Sci. U.S.A.* **92**, 11140–11144 (1995).
12. E. V. Pestova, L. S. Håvarstein, D. A. Morrison, Regulation of competence for genetic transformation in *Streptococcus pneumoniae* by an auto-induced peptide pheromone and a two-component regulatory system. *Mol. Microbiol.* **21**, 853–862 (1996).
13. L. Fontaine *et al*., A novel pheromone quorum-sensing system controls the development of natural competence in *Streptococcus thermophilus* and *Streptococcus salivarius*. *J. Bacteriol.* **192**, 1444–1454 (2010).
14. L. Fontaine *et al*., Mechanism of competence activation by the ComRS signalling system in streptococci. *Mol. Microbiol.* **87**, 1113–1132 (2013).
15. R. Gardan *et al*., Extracellular life cycle of ComS, the competence-stimulating peptide of *Streptococcus thermophilus*. *J. Bacteriol.* **195**, 1845–1855 (2013).
16. L. Mashburn-Warren, D. A. Morrison, M. J. Federle, A novel double-tryptophan peptide pheromone controls competence in *Streptococcus* spp. via an Rgg regulator. *Mol. Microbiol.* **78**, 589–606 (2010).
17. J. Mignolet *et al*., Circuitry rewiring directly couples competence to predation in the gut dweller *Streptococcus salivarius*. *Cell Rep.* **22**, 1627–1638 (2018).
18. N. Declerck *et al*., Structure of PlcR: Insights into virulence regulation and evolution of quorum sensing in Gram-positive bacteria. *Proc. Natl. Acad. Sci. U.S.A.* **104**, 18490–18495 (2007).
19. M. B. Neiditch, G. C. Capodagli, G. Prehna, M. J. Federle, Genetic and structural analyses of RRNPP intercellular peptide signaling of Gram-positive bacteria. *Annu. Rev. Genet.* **51**, 311–333 (2017).
20. L. D. D'Andrea, L. Regan, TPR proteins: The versatile helix. *Trends Biochem. Sci.* **28**, 655–662 (2003).
21. R. Wintjens, M. Rooman, Structural classification of HTH DNA-binding domains and protein-DNA interaction modes. *J. Mol. Biol.* **262**, 294–313 (1996).
22. I. B. Wenderska *et al*., A novel function for the competence inducing peptide, XIP, as a cell death effector of *Streptococcus mutans*. *FEMS Microbiol. Lett.* **336**, 104–112 (2012).
23. R. Khan *et al*., Extracellular identification of a processed type II ComR/ComS pheromone of *Streptococcus mutans*. *J. Bacteriol.* **194**, 3781–3788 (2012).
24. E. Shanker *et al*., Pheromone recognition and selectivity by ComR proteins among *Streptococcus* species. *PLoS Pathog.* **12**, e1005979 (2016).
25. A. Talagas *et al*., Structural insights into streptococcal competence regulation by the cell-to-cell communication system ComRS. *PLoS Pathog.* **12**, e1005980 (2016).
26. L. Fontaine *et al*., Development of a versatile procedure based on natural transformation for marker-free targeted genetic modification in *Streptococcus thermophilus*. *Appl. Environ. Microbiol.* **76**, 7870–7877 (2010).
27. S. Nessler, J. Thuillier, L. Ledesma, P. Hols. Apo form of the competence regulator ComR from *Streptococcus vestibularis*. Protein Data Bank. https://www.rcsb.org/structure/6HU8. Deposited 5 October 2018.
28. S. Nessler, J. Thuillier, L. Ledesma, P. Hols. The competence regulator ComR from *Streptococcus vestibularis* in complex with its cognate signaling peptide XIP. Protein Data Bank. https://www.rcsb.org/structure/6HUA. Deposited 5 October 2018.
29. N. Zeytuni, R. Zarivach, Structural and functional discussion of the tetra-trico-peptide repeat, a protein interaction module. *Structure* **20**, 397–405 (2012).
30. J. Thuillier, S. Nessler, Apo Form Of ComR from *S. thermophilus* in space group C2. Protein Data Bank. https://www.rcsb.org/structure/6QER. Deposited 8 January 2019.
31. W. Kabsch, Xds. *Acta Crystallogr. D Biol. Crystallogr.* **66**, 125–132 (2010).
32. A. J. McCoy *et al*., Phaser crystallographic software. *J. Appl. Cryst.* **40**, 658–674 (2007).
33. P. D. Adams *et al*., PHENIX: A comprehensive python-based system for macromolecular structure solution. *Acta Crystallogr. D Biol. Crystallogr.* **66**, 213–221 (2010).
34. P. Emsley, K. Cowtan, Coot: Model-building tools for molecular graphics. *Acta Crystallogr. D Biol. Crystallogr.* **60**, 2126–2132 (2004).
35. E. Krissinel, K. Henrick, Inference of macromolecular assemblies from crystalline state. *J. Mol. Biol.* **372**, 774–797 (2007).
36. E. Krissinel, K. Henrick, Secondary-structure matching (SSM), a new tool for fast protein structure alignment in three dimensions. *Acta Crystallogr. D Biol. Crystallogr.* **60**, 2256–2268 (2004).
37. R. A. Laskowski, M. B. Swindells, LigPlot+: Multiple ligand-protein interaction diagrams for drug discovery. *J. Chem. Inf. Model.* **51**, 2778–2786 (2011).